Nonlinear Dynamic Analysis of Coupled Gear-Rotor-Bearing System with the Effect of Internal and External Excitations

ZHOU Shihua, SONG Guiqiu*, REN Zhaohui, and WEN Bangchun

School of Mechanical Engineering and Automation, Northeastern University, Shenyang 110819, China

Abstract: Extensive studies on nonlinear dynamics of gear systems with internal excitation or external excitation respectively have been carried out. However, the nonlinear characteristics of gear systems under combined internal and external excitations are scarcely investigated. An eight-degree-of-freedom(8-DOF) nonlinear spur gear-rotor-bearing model, which contains backlash, transmission error, eccentricity, gravity and input/output torque, is established, and the coupled lateral-torsional vibration characteristics are studied. Based on the equations of motion, the coupled spur gear-rotor-bearing system(SGRBS) is investigated using the Runge-Kutta numerical method, and the effects of rotational speed, error fluctuation and load fluctuation on the dynamic responses are explored. The results show that a diverse range of nonlinear dynamic characteristics such as periodic motion, quasi-periodic motion, chaotic behaviors and impacts exhibited in the system are strongly attributed to the interaction between internal and external excitations. Significantly, the changing rotational speed could effectively control the vibration of the system. Vibration level increases with the increasing error fluctuation. Whereas the load fluctuation has an influence on the nonlinear dynamic characteristics and the increasing excitation force amplitude makes the vibration amplitude increase, the chaotic motion may be restricted. The proposed model and numerical results can be used for diagnosis of faults and vibration control of practical SGRBS.

Keywords: spur gear-rotor-bearing system(SGRBS), backlash, eccentricity, internal and external excitations, coupled lateral-torsional vibration

1 Introduction

Gear transmission system, as one of the most common types of rotating machinery which is quite extensive used in wind turbines, ships, automobiles, and aircrafts, plays an important role in industrial application. However, the severe working environment often inevitably causes the gear system break down, and even results in significant economic losses and catastrophic accidents. Therefore, accurately detecting the dynamic behaviors of the gear system is a great significance for avoiding serious aftereffects and ensuring the safe and stable operation of the mechanical equipment. A great number of theoretical researches have been carried out in order to reveal the dynamic behaviors of the gear transmission system. In recent years, with the increased demand for high speed, high flexibility and high efficiency, many researchers have made a great contribution to study dynamic characteristics of gear systems by applying experimental methods, numerical simulation technique and analytical methods,

respectively. The coupled of gears, shafts and bearings usually simplified to single-degree-of-freedom(SDOF) model or multi-degree-of-freedom(MDOF) model, which include time-varying parameters and nonlinear features. These models can be used to analyze the influences on gear modification, mounting error, clearance in gear system.

In earlier studies, the spur gear system was usually analyzed by SDOF. KAHARMAN, et al[1], studied the nonlinear dynamic characteristics of spur gear system with the harmonic balance method(HBM). In order to further study the nonlinear characteristics of gear transmission system, KAHARMAN[2] sequentially analyzed the effect of the gear rotor-bearing system with the backlash and the time-varying mesh stiffness, and carried out a detailed analysis to the nonlinear system. LI, et al[3], established a SDOF gear pair model with internal and external periodic excitations, and the key parameters of dynamic backlash, damping ratio and the excitation force amplitude were analyzed by incremental harmonic balance method(IHBM). BARBIERI, et al[4], applied genetic algorithms for optimizing spur gear in terms of static transmission ratio, the procedure considered a nonlinear finite element analysis for the evaluation of the transmission error within the optimization algorithm. BONORI, et al[5], presented a method for analyzing nonlinear vibration of gear system in presence of manufacturing errors, which used a SDOF

• 282 •

ZHOU Shihua, et al: Nonlinear Dynamic Analysis of Coupled Gear-Rotor-Bearing System
with the Effect of Internal and External Excitations

dynamic model to check the efficiency in terms of vibration reduction of the optimized profile reliefs.

However, the observed phenomena indicate that support bearing, gear eccentricity and backlash make the system have strong nonlinearity, the SDOF model will fail to reflect the nonlinear dynamic behaviors of the SGRBS when the perturbed motion of bearing and the vibration of housing are no longer small. Based on both SDOF and MDOF models, CHEN, et al[6], established a MDOF gear system with the effect of the friction and dynamic backlash, and the impact motion was predicted. ZHOU, et al[7], studied the nonlinear characteristics of gear transmission system under the action of external and internal excitations by the IHBM, and the vibration response obtained by IHBM compared very well with the results obtained by Newmark method. WEI, et al[8] investigated the dynamic responses of a torsional vibration geared system with uncertain parameters by using the Chebyshev interval method. ZHU, et al[9], used the HBM to investigate the nonlinear dynamics of a compound planetary gear sets, and the effects of nonlinearities on the frequency response characteristics were investigated by changing parameters. WAN, et al[10] presented a series of investigations to the dynamic behaviors of gear-bearing system with nonlinear suspension, nonlinear oil-film force and nonlinear gear mesh force, and the results provided an understanding of the operating conditions under which undesirable dynamic motion took place in a gear bearing system. MA, et al[11–12] established a finite element model of a cracked gear coupled rotor system in a one-stage reduction gearbox and the effects of crack depth, width, initial position and crack propagation direction on gear mesh stiffness, fault features in time domain, frequency domain and statistical indicators were investigated. FAGGIONI, et al[13], presented a global optimization method focused on gear vibration reduction by means of profile modification, which reduced the vibration over a wide range of operating conditions and the optimum reliability was estimated using a Monte Carlo simulation. LEE, et al[14], studied the coupled vibration characteristics of a turbo-chiller rotor-bearing system having a bull-pinion speed increasing gear, and provided the mechanism of the characteristic changes. YASSINE, et al[15], analyzed a three-dimensional model of two-stage straight bevel gear system, and some defects in the developed model such us the eccentricity defect, profile error and cracked tooth were introduced. HUANG, et al[16], developed a time-varying model considering the mesh stiffness, damping factor, mesh force and frictional force between the tooth pairs at each calculation step, and the effects of the lubricant viscosity and applied torque on the gear dynamics were thoroughly studied. STRINGER, et al[17], studied a methodology for conducting modal reduction on a gear rotor dynamic system under the influences of general damping and gyroscopic effects, and widely discussed eigen-solution analysis. HE, et al[18], developed spur gear rotor model with sliding friction and

rectangular mesh stiffness by assuming that load was equally shared among all the teeth in contact, and solved the gear system equations by using the Floquet theory and the HBM. PAREY, et al[19], established a dynamic model including localized tooth defect, and the processing of simulated and experimental signals were proposed in order to analyze nonstationary and nonlinear characteristics. OMAR, et al[20], presented a dynamic model taking into account gear size, errors and faults, and used parameters representing a real experimental gearbox rig. In addition, experimental and simulated data were compared for different operating speeds, torque loads and gear cracks. HOTAIT, et al[21], described a gear dynamics test set-up with integrated root strain and dynamic transmission error measurement systems, and dynamic factor and dynamic transmission error measurements from unmodified and modified spur gears were presented. TAMMINANA, et al[22], developed two different dynamic models, a finite-element-based deformable-body model and a simplified discrete model, to predict dynamic behavior of spur gear pairs, and the impact of nonlinear behaviors, such as tooth separations and jump discontinuities were quantified. AMARNATH, et al[23], conducted experimental investigations on the measurement of reduction in the gear teeth stiffness along with vibration parameters, and experimental measurement of stiffness was carried out using modal analysis in conjunction with a theoretical model. LEE, et al[24], presented an experimental investigations carried out to assess the surface fatigue wear in a spur gear system. The estimation of specific film thickness, measurement of reduction in tooth thickness, visual examination of wear mechanisms on the gear teeth and their effects on the statistical parameters of vibration and sound signals were considered. WANG, et al[25], proposed a new method of modified optimization of double helical gears based on reducing vibration and noise and raising machining efficiency, and the test-bed of vibration and noise were designed. RAFIQ, et al[26], analyzed a new nonlinear dynamic model, which was coupled with linear finite element models of shafts carrying them, and with discrete models of bearings and disks. The results were compared with the experimental data available. MA[27–28] investigated the dynamic behaviors of a perforated gear system considering effects of the gear crack propagation paths and focused on the effects of a crack propagating through the rim on the time-varying mesh stiffness and vibration responses. MOHMMED, et al[29], modelled a one-stage reduction gear using three different dynamic models (with 6, 8 and 8 reduced to 6 DOF), as well as the developed model (with 12 DOF). The dynamic simulation was performed for different crack sizes, and time domain scalar indicators were applied for fault detection analysis. HU, et al[30], proposed a 14-DOF lumped parameter dynamic model considering coupled multi-body dynamics of the face geared rotor system with coupled translation-rotation vibration. And the jump phenomenon,

periodic window, doubling-periodic bifurcation and chaotic behavior of the system were observed. ZHOU, et al[31], developed calculation of the contact position, impact velocity, impact force and impact friction coefficient. The "gear equivalent error-combined deformation" model was constructed by combining with gear error, deformation and load effect.

Dynamic models of gear systems with flexible shafts and bearings have been investigated by many researchers. The models in the literature are complexity but most of them do not consider the gravity and impact motion in the simulations. In order to clearly understand the dynamic behaviors, a detailed analysis of vibration characteristics with complex model and analysis considering gravity, backlash, especially the fluctuation of drive load, and eccentricity should be given a deeper insight into gear dynamic characteristics. The proposed 8-DOF lateral and torsional generalized lumped parameter model of spur gear system is used to more precisely examine the coupled vibration characteristics of the SGRBS, which is the partial of wind turbine gearbox. Moreover, a comprehensive physical parametric study is accomplished to evaluate the effects of various dynamic parameters such as rotational speed, error fluctuation and load fluctuation.

The rest of this paper organized as follows: In section 2, the mathematical model of a SGRBS combing with 8-DOF is proposed. In section 3, parametric studies are performed for several designing and working parameters in order to quantify their influence on the overall behaviors of the SGRBS. In the last section, some conclusions are presented.

2 Dynamic Model and Equations of Motion

2.1 Model of the SGRBS

In order to efficiently study the dynamic behaviors of the SGRBS, a simplified 8-DOF coupled lateral-torsional generalized lumped parameter model consists of driving and driven gears, drive and load in Fig. 1.

In Fig. 1(b), the mesh relationship between driving gear and driven gear is represented using mesh stiffness k_m and damping c_m elements acting along the line of action. This line of action is defined as the common tangent line of the base circles in the gears having involute tooth form. All supports/bearings are modeled as springs and dampings. In addition, friction forces due to gear teeth contact and other dissipative effects are captured using damping. The gears are represented by base circles with radius r_{b1} and r_{b2}, respectively. m_1 and m_2 indicate the masses of the gears. J_1 and J_2 represent the moment of inertia of gears. The eccentricities for the gears are denoted by ρ_1 and ρ_2, respectively. The gear mesh has a constant backlash $2b$ along the line of action. O_1 and O_2 are the centers of driving and driven gears when they are rotating. G_1 and G_2

represent the centers of mass. The coupled connections between shafts, and the drive/load are modeled as torsional stiffnesses and dampings. k_{xi}, k_{yi} and k_{ti} ($i=1$, 2) are the equivalent lateral and torsional stiffnesses of shafts and bearings, respectively. c_{xi}, c_{yi} and c_{ti} ($i=1$, 2) are the equivalent lateral and torsional dampings of shafts and bearings.
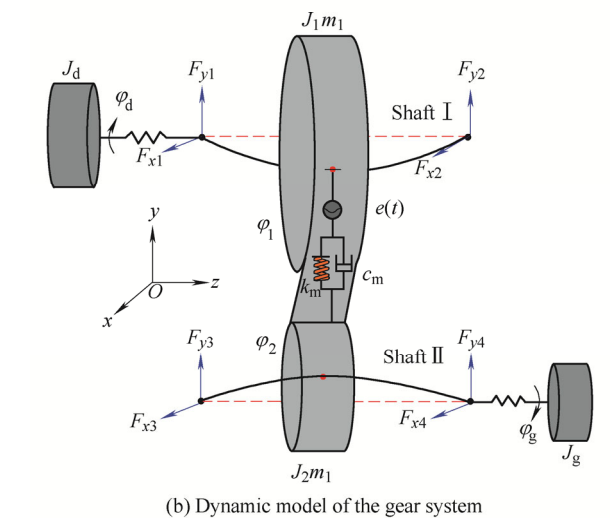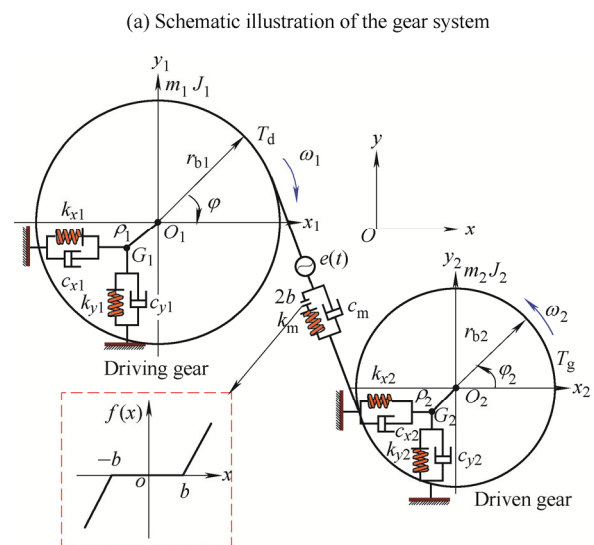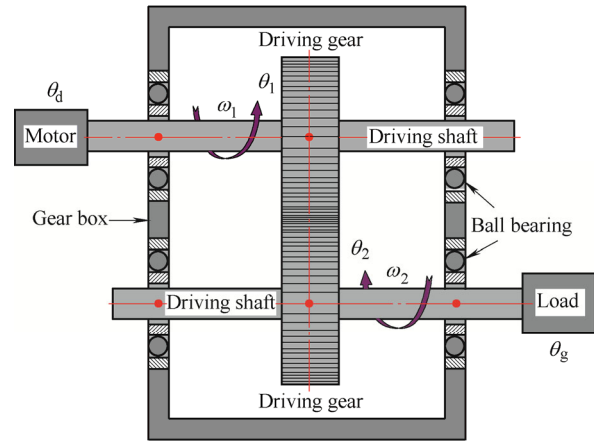

(a) Schematic illustration of the gear system

(b) Dynamic model of the gear system

Fig. 1. Dynamic model of coupled lateral-torsional of SGRBS

The torsional angular displacement of gears, drive and

• 284 •

ZHOU Shihua, et al: Nonlinear Dynamic Analysis of Coupled Gear-Rotor-Bearing System
with the Effect of Internal and External Excitations

load are assumed to result from a constant angular velocity term $\omega_i t$ ($i=1, 2$) plus a small variation displacement $\theta_i(t)$ ($i=$d, 1, 2, g) due to vibration originating from the flexibility of shafts, backlash and drive/load fluctuation. Therefore, the angle displacements $\varphi_i(t)$ ($i=$d, 1, 2, g) of the gears and input/output can be expressed as follows:

$$\varphi_{\mathrm{d}} = \omega_1 t + \theta_{\mathrm{d}}, \varphi_1 = \omega_1 t + \theta_1,$$
$$\varphi_2 = \omega_2 t + \theta_2, \varphi_{\mathrm{g}} = \omega_2 t + \theta_{\mathrm{g}}. \tag{1}$$

Due to the existence of eccentricity, the centers of rotational $O_1(x_1, y_1)$, $O_2(x_2, y_2)$ and the centers of mass $G_1(x_{\mathrm{g}1}, y_{\mathrm{g}1})$, $G_2(x_{\mathrm{g}2}, y_{\mathrm{g}2})$ are misalignment. Therefore, the relationship between them can be expressed as follows:

$$x_{\mathrm{g}1} = x_1 + \rho_1 \cos(-\varphi_1), y_{\mathrm{g}1} = y_1 + \rho_1 \sin(-\varphi_1),$$
$$x_{\mathrm{g}2} = x_2 + \rho_2 \cos\varphi_2, y_{\mathrm{g}2} = y_2 + \rho_2 \sin\varphi_2. \tag{2}$$

According to the mesh relationship, displacement $\delta(t)$ along the line of action can be written:

$$\delta(t) = (r_{\mathrm{b}1}\varphi_1 - r_{\mathrm{b}2}\varphi_2) + (x_{\mathrm{g}1} - x_{\mathrm{g}2})\sin\alpha +$$
$$(y_{\mathrm{g}1} - y_{\mathrm{g}2})\cos\alpha - e(t). \tag{3}$$

Substituting Eq. (2) into Eq. (3), the displacement $\delta(t)$ can be represented as follows:

$$\delta(t) = (r_{\mathrm{b}1}\theta_1 - r_{\mathrm{b}2}\theta_2) +$$
$$(x_1 - x_2 + \rho_1 \cos(-\varphi_1) - \rho_2 \cos\varphi_2)\sin\alpha +$$
$$(y_1 - y_2 + \rho_1 \sin(-\varphi_1) - \rho_2 \sin\varphi_2)\cos\alpha - e(t), \tag{4}$$

where α is the pressure angle of the gears; $e(t)$ represents the static transmission error, which is the high-frequency caused by manufacturing and installation errors. $e(t)=e_{\mathrm{m}}+e_{\mathrm{r}}\sin(\omega_{\mathrm{m}}+\varphi_{\mathrm{m}})$, e_{m} represents the mean and e_{r} indicates the fluctuation, respectively. φ_{m} represents the initial phase angle, then $\omega_{\mathrm{m}}=2\pi n_1 z_1/60 =2\pi n_2 z_2/60$ is the mesh angular frequency, z_1 and z_2 are the number of teeth of driving and driven gears. n_1 and n_2 indicate the rotational speed of the driving and driven gears.

The dynamic mesh force acting on the mesh point is

$$F_{\mathrm{m}} = c_{\mathrm{m}}\dot{\delta} + k_{\mathrm{m}}f(\delta), \tag{5}$$

where $c_{\mathrm{m}} = 2\xi_{\mathrm{m}}\sqrt{k_{\mathrm{m}}/[(1/m_1) + (1/m_2)]}$, ξ_{m} is the damping ratio. $f(\delta)$ is the backlash function in the nonlinear gear system can be represented as follows:

$$f(\delta) = \begin{cases} \delta - b, & \delta > b, \\ 0, & -b < \delta < b, \\ \delta + b, & \delta < -b. \end{cases} \tag{6}$$

The backlash function $f(\delta)$ is shown in Fig. 2. According

to the backlash function $f(\delta)$[32], the impact is not observed in a gear system when the displacement δ lies in the region $\delta_{\max}<b$ and $\delta_{\min}>-b$, which is shown in Fig. 2 as case I. Double-sided impact case exists when the displacement δ lies in the region $\delta_{\max}>b$ and $\delta_{\min}<-b$ and illustration of double-sided impact case III is shown in Fig. 2. When the displacement δ lies in the region $\delta_{\max}>b$ and $\delta_{\min}>-b$ or $\delta_{\max}<b$ and $\delta_{\min}<-b$, the system presents single-sided impact case II. When the system exists the impacts, which include the double-sided impact and single-side impact, the gear system presents an unstable motion state.

In order to simplify the nonlinear problem, the output torque is usually assumed to be constant and neglect the fluctuation in the previous literature. Actually, the output torque also exists fluctuation. Therefore, the input/output torque $T_i(t)$ ($i=$d, g) can be decomposed into mean T_{im} and perturbation $T_{ir}(t)$ parts. This is due to the SGRBS is a part of wind turbine gearbox, it essentially fluctuates between low and high values around the stochastic nature of wind speed. T_{d} and T_{g} are input and output torques acting on the driving and driven gears, respectively. Therefore, the input/output torque can be written:

$$T_{\mathrm{d}} = T_{\mathrm{dm}} + T_{\mathrm{dr}}\sin(\omega_1 t + \varphi_{\mathrm{d}}),$$
$$T_{\mathrm{g}} = T_{\mathrm{gm}} + T_{\mathrm{gr}}\sin(\omega_2 t + \varphi_{\mathrm{g}}), \tag{7}$$

where T_{dm} and T_{gm} are the means, T_{dr} and T_{gr} represent the fluctuations, $\omega_i=2\pi n_i/60$ is the rotational frequency, φ_{d} and φ_{g} represent the initial phase angles.
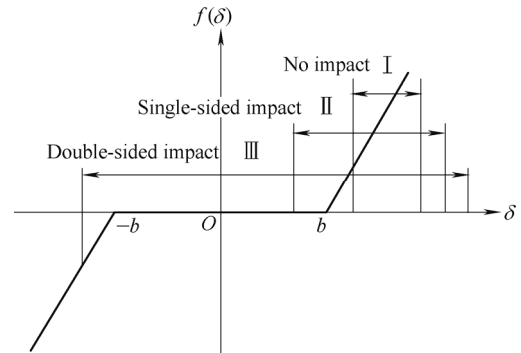

Fig. 2. Backlash function

2.2 Equations of motion

In this section, the motion differential equations of the SGRBS are derived. The nonlinear system has eight degrees of freedom about frame X-Y-Θ, including four laterals of mass center (x_1, y_1, x_2 and y_2,) and four rotations of the plane of the gears and drive/load (θ_{d}, θ_1, θ_2 and θ_{g}). Therefore, the generalized coordinate vector of the nonlinear dynamic model can be expressed as follows:

$$\boldsymbol{X} = [\theta_{\mathrm{d}} \quad x_1 \quad y_1 \quad \theta_1 \quad x_2 \quad y_2 \quad \theta_2 \quad \theta_{\mathrm{g}}]^{\mathrm{T}}. \tag{8}$$

The kinetic energy T, potential energy U and dissipation

function R of the SGRBS can be expressed as follows:

$$T = \frac{1}{2}\Big(m_1 x_{g1}^2 + m_1 y_{g1}^2 + m_2 x_{g2}^2 + m_2 y_{g2}^2 +$$
$$J_d \dot{\varphi}_d^2 + J_1 \dot{\varphi}_1^2 + J_2 \dot{\varphi}_2^2 + J_g \dot{\varphi}_g^2\Big),$$

$$U = \frac{1}{2}\Big[\big(k_{sx1} x_1^2 + k_{sy1} y_1^2 + k_{sx2} x_2^2 + k_{sy2} y_2^2\big) +$$
$$k_{t1}\big(\varphi_1 - \varphi_d\big)^2 + k_{t2}\big(\varphi_g - \varphi_2\big)^2\Big],$$

$$R = \frac{1}{2}\Big[\big(k_{sx1}\dot{x}_1^2 + k_{sy1}\dot{y}_1^2 + k_{sx2}\dot{x}_2^2 + k_{sy2}\dot{y}_2^2\big) +$$
$$k_{t1}\big(\dot{\varphi}_1 - \dot{\varphi}_d\big)^2 + k_{t2}\big(\dot{\varphi}_g - \dot{\varphi}_2\big)^2\Big].$$

$$(9)$$

The force vector $\boldsymbol{F}$ of the SGRBS can be represented by

$$\boldsymbol{F} = [T_d \quad 0 \quad -m_1 g \quad 0 \quad 0 \quad -m_2 g \quad 0 \quad -T_g]^T.$$

$$(10)$$

The vibration differential equations are derived using Lagrange's equation, which is given by

$$\frac{\partial}{\partial t}\left(\frac{\partial T}{\partial \dot{X}}\right) - \frac{\partial T}{\partial X} + \frac{\partial U}{\partial X} + \frac{\partial R}{\partial \dot{X}} = \boldsymbol{F}.$$

$$(11)$$

Substitution Eqs. (8)–(10) into Eq. (11), the mathematical model of SGRBS can be written in matrix form as

$$\boldsymbol{M}\ddot{\boldsymbol{X}} + \boldsymbol{C}\dot{\boldsymbol{X}} + \boldsymbol{K}\boldsymbol{X} = \boldsymbol{F}_L + \boldsymbol{F}_N,$$

$$(12)$$

where $\boldsymbol{M}$, $\boldsymbol{C}$ and $\boldsymbol{K}$ are the mass matrix, damping matrix and stiffness matrix, respectively. $\boldsymbol{F}_L$ is the linear factor vector, and $\boldsymbol{F}_N$ is the nonlinear factor vector. It should be noted that the linear factor vector $\boldsymbol{F}_L$ includes the input torque, output torque and gravity. The nonlinear force vector $\boldsymbol{F}_N$ is a function of the displacement vector $\boldsymbol{X}$, the velocity vector $\dot{\boldsymbol{X}}$ and eccentricity ρ.

$$\boldsymbol{M} = \mathrm{diag}[J_d \quad m_1 \quad m_1 \quad J_1 + m_1 \rho_1^2$$
$$m_2 \quad m_2 \quad J_2 + m_2 \rho_2^2 \quad J_g],$$

$$\boldsymbol{C} = \begin{pmatrix} c_{t1} & 0 & 0 & -c_{t1} & 0 & 0 & 0 & 0 \\ 0 & c_{x1} & 0 & 0 & 0 & 0 & 0 & 0 \\ 0 & 0 & c_{y1} & 0 & 0 & 0 & 0 & 0 \\ -c_{t1} & 0 & 0 & c_{t1} & 0 & 0 & 0 & 0 \\ 0 & 0 & 0 & 0 & c_{x2} & 0 & 0 & 0 \\ 0 & 0 & 0 & 0 & 0 & c_{y2} & 0 & 0 \\ 0 & 0 & 0 & 0 & 0 & 0 & c_{t2} & -c_{t2} \\ 0 & 0 & 0 & 0 & 0 & 0 & -c_{t2} & c_{t2} \end{pmatrix},$$

$$\boldsymbol{K} = \begin{pmatrix} k_{t1} & 0 & 0 & -k_{t1} & 0 & 0 & 0 & 0 \\ 0 & k_{x1} & 0 & 0 & 0 & 0 & 0 & 0 \\ 0 & 0 & k_{y1} & 0 & 0 & 0 & 0 & 0 \\ -k_{t1} & 0 & 0 & k_{t1} & 0 & 0 & 0 & 0 \\ 0 & 0 & 0 & 0 & k_{x2} & 0 & 0 & 0 \\ 0 & 0 & 0 & 0 & 0 & k_{y2} & 0 & 0 \\ 0 & 0 & 0 & 0 & 0 & 0 & k_{t2} & -k_{t2} \\ 0 & 0 & 0 & 0 & 0 & 0 & -k_{t2} & k_{t2} \end{pmatrix},$$

$$\boldsymbol{F}_L = \mathrm{diag}[T_d \quad 0 \quad -m_1 g \quad 0 \quad 0 \quad -m_2 g \quad 0 \quad T_g],$$

$$\boldsymbol{F}_N = \begin{pmatrix} 0 \\ m_1 \rho_1 \dot{\varphi}_1^2 \cos\varphi_1 + m_1 \rho_1 \ddot{\theta}_1 \sin\varphi_1 - F_m \sin\alpha \\ m_1 \rho_1 \dot{\varphi}_1^2 \sin\varphi_1 - m_1 \rho_1 \ddot{\theta}_1 \cos\varphi_1 - F_m \cos\alpha \\ m_1 \rho_1 \ddot{x}_1 \sin\varphi_1 - m_1 \rho_1 \ddot{y}_1 \cos\varphi_1 - F_m r_{b1} \\ m_2 \rho_2 \dot{\varphi}_2^2 \cos\varphi_2 + m_2 \rho_2 \ddot{\theta}_2 \sin\varphi_2 + F_m \sin\alpha \\ m_2 \rho_2 \dot{\varphi}_2^2 \sin\varphi_2 - m_2 \rho_2 \ddot{\theta}_2 \cos\varphi_2 + F_m \cos\alpha \\ m_2 \rho_2 \ddot{x}_2 \sin\varphi_2 - m_2 \rho_2 \ddot{y}_2 \cos\varphi_2 + F_m r_{b2} \\ 0 \end{pmatrix}.$$

3　Dynamic Response of Gear System

From the previous calculation and analysis, it can be seen that the SGRBS is a complicated system with strong nonlinearity and time variance. Therefore, it is necessary to give a detailed analysis of the gear system. The dynamic characteristics of system are investigated by Runge-Kutta. The key parameters are analyzed to obtain a basic understanding the dynamic behaviors of the SGRBS. Table 1 summarizes the geometrical and physical parameters of spur gear. Let rotational speed ω, error fluctuation e_r and load fluctuation T_{dr} be control parameters in the following analysis.

Table 1.　Parameters of the SGRBS

Parameter	Value
Number of teeth z_1, z_2	20
Radius r_{b1}, r_{b2}/m	0.1
Mass m_1, m_2/kg	100.0
Moment of inertia J_1, J_2/(kg · m²)	1.0
Moment of inertia J_d, J_g/(kg · m²)	0.3
Pressure angle α/(°)	20
Mesh stiffness k_m/(MN · m⁻¹)	500
Mesh damping c_m/(kN · m⁻¹ · s⁻¹)	1.2
Eccentricity ρ_1, ρ_2/μm	15
Torsional stiffness k_{t1}, k_{t2}/(MN · m⁻¹ · rad⁻¹)	9.0
Torsional damping c_{t1}, c_{t2}/(N · rad⁻¹ · s⁻¹)	400
Lateral stiffness $k_{x1, y1}$, $k_{x2, y2}$/(MN · m⁻¹)	100
Lateral damping $c_{x1, y1}$, $c_{x2, y2}$/(N · m⁻¹ · s⁻¹)	500
Error mean e_m/μm	20
Error fluctuation e_r/μm	30
Torque mean T_{dm}, T_{gm}/(N · m⁻¹)	400
Torque fluctuation T_{dr}, T_{gr}/(N · m⁻¹)	300
Backlash b/μm	40

• 286 •

ZHOU Shihua, et al: Nonlinear Dynamic Analysis of Coupled Gear-Rotor-Bearing System
with the Effect of Internal and External Excitations

3.1 Model validation

Although many models have been developed in the previous literature, very few considers input/output torque, gravity and eccentricity of the model, which lead to obviously different dynamic characteristics. In order to illustrate the accuracy of the SGRBS, the gear system is simulated by four lumped mass points, Fig. 3 shows the time-domain waveforms in torsional and lateral directions. The results show that there are obvious difference between the vibration response obtained at output terminal and gear. It is clearly that the θ_d is obviously larger than that of θ_1 by comparing the time-domain waveforms of the Fig. 3(a). The phenomenon is caused by the fluctuation of input torque of the system and the vibration transfer gradually reduced. Fig. 3(b) shows the waveforms in x direction and y-direction. Due to the effects of gravity and mounting position, the vibration amplitude in y direction is far greater than one in x-direction. Therefore, the dynamic model of SGRBS considering the input/output, gravity and mounting position is necessary.
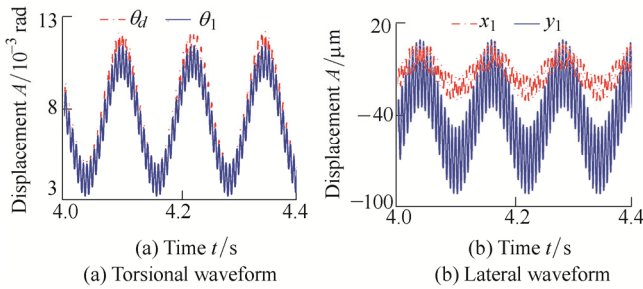

(a) Time t/s
(a) Torsional waveform

(b) Time t/s
(b) Lateral waveform

Fig. 3.　Time-domain waveform of the SGRBS at ω=500 r/min

3.2 Analysis of the effect of the rotational speed

The piecewise nonlinear system with periodical parameters have attracted significant attention. In practical SGRBS, the rotational speed ω is commonly used as a control parameter. Accordingly, this section devotes itself to studying the effect on the rotational speed of the dynamic responses with the 8-DOF SGRBS, and only the stable solutions are shown here. Because the vibration response of the driving/driven gear exhibits the similar form of motion, the driving gear vibration responses are taken for example.

Keeping all other parameters unchanged, taking the rotational speed ω as the control parameters, the vibration waveform, the frequency spectrum, the phase diagram and the deformation, under two different rotational speed conditions, low speed 500 r/min and high speed 5000 r/min, are adopted to indicate the dynamic features in Fig. 4 and Fig. 5, respectively. The vibration responses of the SGRBS at low speed 500 r/min are given in Figs. 4(a)–(d). From the figures, it indicates that the two types of harmonic components appear in Fig. 4(a), which possesses two periods T_r (T_r=2π/ω_1=0.12 s) and T_m (T_m=2π/ω_m= 6.0×10^{-3} s), respectively. In addition, the vibration amplitude in x direction of mesh frequency f_m

(f_m=z_1f_r=166.67 Hz) is the second largest after that of the rotational frequency f_r (f_r=n/60=8.33 Hz), and the combination frequency and multiplication frequency components can't be observed, as is shown in Fig. 4(b). At this speed, the phase diagram of the driving gear shows regular motion in Fig. 4(c). The single-sided impact of the system can also be verified by the deformation due to δ_{max}>b and δ_{min}>−b, as shown in Fig. 4(d). Figs. 5(a)–(d) displays the vibration responses of the SGRBS at high speed 5000 r/min. Here, it can be found from Fig. 5(a) that the vibration amplitude obviously higher with increasing speed. However, the frequency components are significant differences at high speed and the frequency components become more complicated, which contains a response peak at frequency 83.33 Hz in addition to response peak at 1666.67 Hz. The multiplication frequency(2f_m, 3f_m), the combination frequency(1.5f_m±f_r, 2f_m±f_r) and fractional frequency(0.5f_m, 1.5f_m) components can be observed in Fig. 5(b). The phase diagram shows slight irregular motion in Fig. 5(c). Due to δ_{max}>b and δ_{min}<−b, the SGRBS lies in double-sided impact.
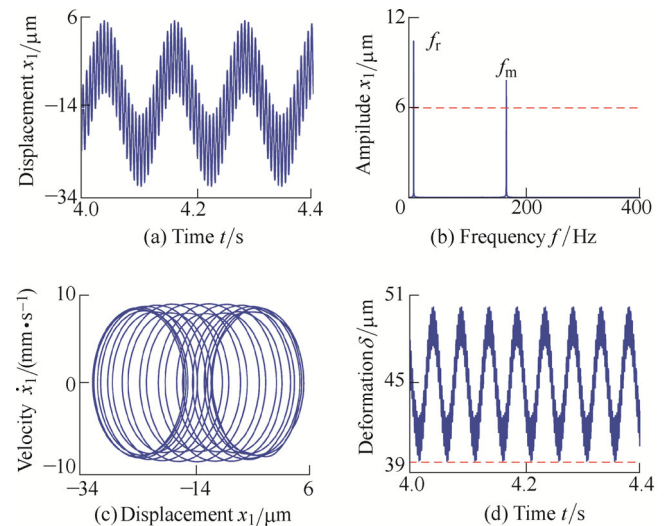

(a) Time t/s

(b) Frequency f/Hz

(c) Displacement x_1/μm

(d) Time t/s

Fig. 4.　Vibration responses of the SGRBS at ω=500 r/min

(a) Time t/s

(b) Frequency f/kHz

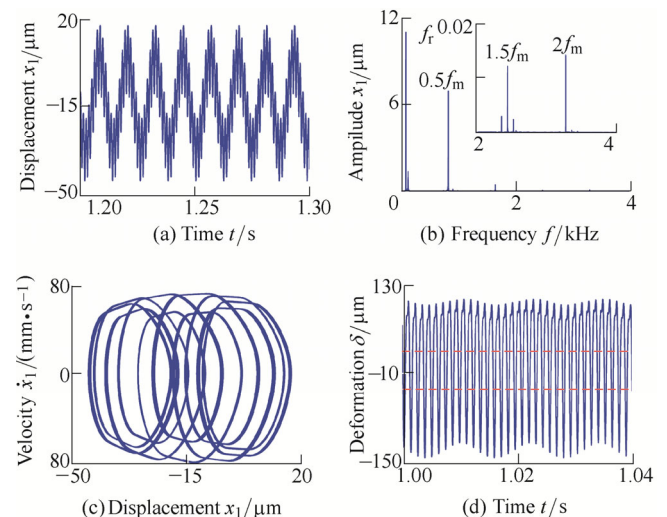(c) Displacement x_1/μm

(d) Time t/s

Fig. 5.　Vibration responses of the SGRBS at ω=5000 r/min

Based on the above analysis, it is clear that the rotational speed ω is an important parameter and affects the dynamic behaviors of the SGRBS. Fig. 6 presents the mesh force of the system at 500 r/min and 5000 r/min. It can be seen that the fluctuation of the dynamic mesh force becomes more apparent and exists significant negative value at high rotational speed. Because the bending deformations increase of the driving and driven gears with the increasing rotational speed, which leads to the mesh impact activation and take off a tooth phenomenon become more apparent. The vibration amplitude significantly larger and vibration intensified.
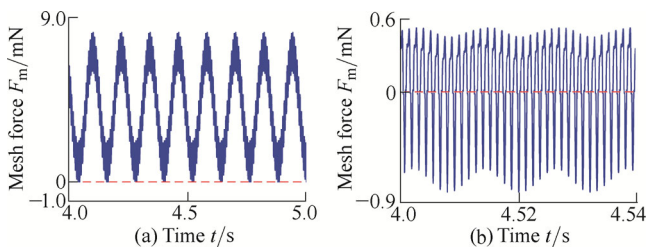

Fig. 6.   Mesh force at $\omega=500$ r/min and $\omega=5000$ r/min

For a better understanding the dynamic characteristics of the SGRBS and the influence on the rotational speed, Fig. 7 presents the 3-D(3-dimensional) frequency spectrum (Fig. 7(a)) and the bifurcation diagram (Fig. 7(b)) with ω as control parameter in the range of $\omega \in [50, 900]$ rad/s. It can be seen that the mesh frequency(f_m) and rotational frequency(f_r) are the main frequency components and other frequency components don't appear. The mesh frequency's amplitude decreases gradually and the amplitude of f_r increases firstly and then decreases at low values of the rotational speed ω, i.e., $\omega \leqslant 100$ rad/s in Fig. 7(a). The nT-periodic motion can be seen as shown in Fig.7(b). However, as ω is increased from 100 rad/s to 165 rad/s, the 3-D frequency spectrum becomes more complex, which exhibits continuous frequency components. The rotational frequency(f_r) is dominated response. The amplitude of f_m steadily increases and the rotational frequency's amplitude keeps the same. The corresponding bifurcation diagram transits to chaotic behaviors. As the rotational speed is further increased from $\omega=165$ rad/s to $\omega=330$ rad/s, the f_r, f_m and multiplication frequency($2f_m$, $3f_m$) appear in 3-D frequency spectrum and combination frequency components are not obvious. Nevertheless, the mesh frequency component reaches to a response peak at $\omega=330$ rad/s, and the amplitude of f_m is considerably larger than other frequency components. In addition, the mesh frequency appears strongly jump discontinuous phenomena. The f_r is not a significant change in amplitude. The bifurcation diagram presents different periodic motions. With the increase of the rotational speed from 330 rad/s to 535 rad/s, the amplitude of f_r increases gradually, but the amplitude of f_m decreases. The 3-D frequency spectrum is from continuous excitation frequency components in the range of $\omega \in [330, 450]$ rad/s to discrete frequency

components in the range of $\omega \in [450, 535]$ rad/s, and the system exhibits nT-periodic through chaotic motion bifurcation. The multiplication frequency($0.5f_m=10f_r$) appears obviously, and the amplitude is the second largest after that of the rotational frequency f_r at $\omega \in [450, 535]$ rad/s. As the control parameter ω is further increased, the rotational frequency f_r is the main response and a continuous frequency components exhibit at $\omega \in [535, 580]$ rad/s, discrete frequency components, such as rotational frequency f_r and multiplication frequency($7f_r$) at $\omega \in [580, 735]$ rad/s. In addition, the amplitude of f_r increases gradually and the mesh frequency's amplitude is not obvious. In the bifurcation diagram, the behavior of system reverts from chaotic motion to quasi-periodic bifurcation. Finally, for all $\omega \geqslant 735$ rad/s, the amplitude of f_r reaches the peak at $\omega \geqslant 775$ rad/s. After that point, the amplitude decreases gradually. The chaotic motion is replaced by quasi-periodic motion. Therefore, it can be concluded that the rotational speed has an influence on the nonlinear dynamic characteristics and the increasing speed can lead to the SGRBS exhibits chaotic behavior, accompanying separation phenomenon and single-sided/doubled-sided impact.
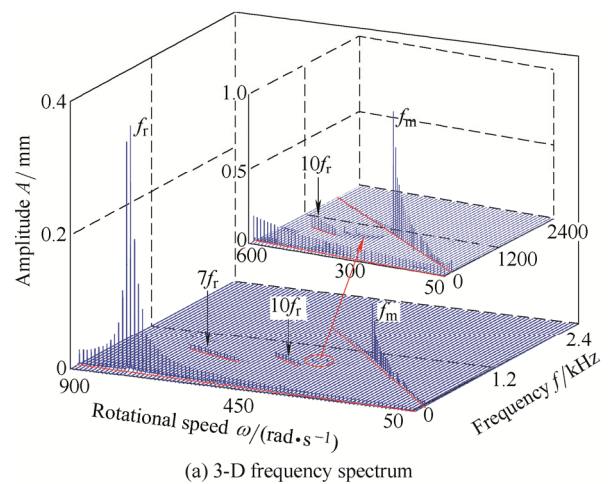
(a) 3-D frequency spectrum
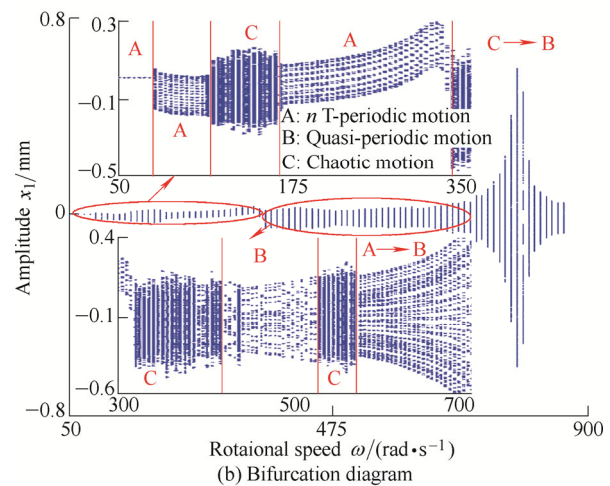
(b) Bifurcation diagram

Fig. 7.   3-D frequency spectrum and bifurcation diagram

3.3   Analysis of the effect of the error fluctuation

In this section, the main purpose is to analyze the effect

• 288 •

ZHOU Shihua, et al: Nonlinear Dynamic Analysis of Coupled Gear-Rotor-Bearing System
with the Effect of Internal and External Excitations

on the error fluctuation in the nonlinear dynamic model of the coupled SGRBS. The transmission error caused by manufacturing error and installation error is a displacement excitation at the mesh point due to the geometrical error of the teeth profile and spacing, which not only affects the vibration amplitude of the system, but also directly affects the degree of nonlinearity. To illustrate the influence on the SGRBS with the error fluctuant amplitude e_r, a further analysis has been carried out considering several set of simulated of the error fluctuant amplitude in Fig. 8(e_r=20 μm) and Fig. 9(e_r=80 μm). It can be seen from Fig. 8(b) that the rotational frequency(f_r) dominated in frequency spectrum, and the phase diagram in Fig. 8(c) exhibits 20 oscillations associated with the tooth number of the gear. The deformation presented in Fig. 8(d) shows that the single-sided impact exists only due to δ_{max}>b and δ_{min}>−b. When e_r is equal to 80 μm, comparing Fig. 8 with Fig. 9, it can be seen from Fig. 9(a) that the vibration displacement in torsional direction significantly larger. In Fig. 9(b), the rotational frequency(f_r) is also the dominated response in frequency spectrum, and the amplitude has an increase. In addition, the multiplication frequency($2f_r$, $3f_r$, $4f_r$, $2f_m$), the combination frequency($f_m \pm f_r$, $2f_m \pm f_r$) and continuous frequency components appear. In Fig. 9(c), the phase diagram shows irregular motion, and the SGRBS undergoes the double-sided impact, as shown in Fig. 9(d).
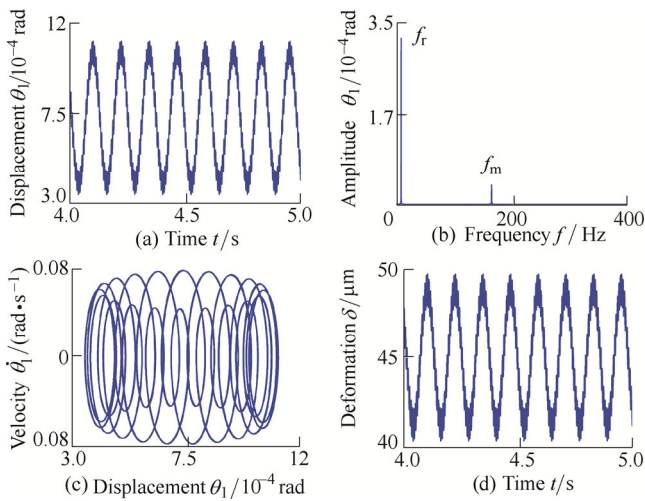

Fig. 9.   Vibration responses of SGRBS at e_r=80 μm

Fig. 10.   Mesh force at e_r=20 μm and e_r=80 μm

Fig. 8   Vibration responses of SGRBS at e_r=2.0×10⁻⁵ m

The dynamic mesh force is also an important evaluation factor of the SGRBS. Fig. 10 presents the mesh force at e_r=20 μm and e_r=80 μm m. Note that the mesh force is almost positive at low values of the error fluctuation and the positive and negative values alternate at high fluctuation. The main reason for this phenomenon is due to the larger fluctuation of the transmission error, which leads to transform of the gear mesh state and separation phenomenon. The driving gear is impacted repeatedly with higher dynamic load by the driven gear due to the separation phenomenon. Therefore, the nonlinear degree of the dynamic mesh force is significantly higher with increasing error fluctuation.
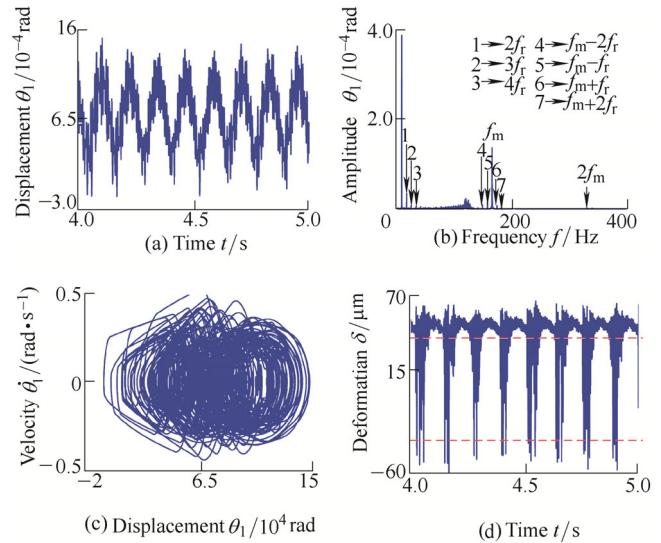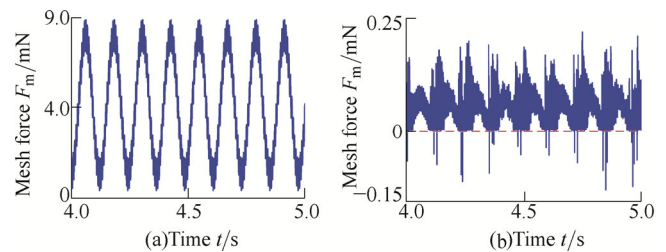
The vibration responses of the SGRBS in the range of e_r ∈ [10, 500] μm are studied and the 3-D frequency spectrum(Fig. 11(a)) and the bifurcation diagram(Fig. 11(b)) of the rotational direction(θ_1) using e_r as control parameter are given in Fig. 11. The dynamic responses of the system exhibit different nonlinear phenomena with changing e_r. It can be observed that the SGRBS exhibits two types of frequency components(f_r, f_m) at low values of the error fluctuation, i.e., $e_r \leqslant 30$ μm. In addition, the rotational frequency is the dominated response and the amplitude of f_r remains about the same, the mesh frequency's amplitude increases gradually. Other frequency components don't appear in the 3-D frequency spectrum. It can be found from Fig. 11(b) that there is only quasi-periodic motion. However, with the increase of the control parameter e_r, the f_r and f_m are the dominated responses. The multiplication frequency($2f_r$, $3f_r$, $2f_m$···) and the combination frequency ($f_m \pm f_r$) components can be observed. The continuous frequency components are becoming more apparent, which are mainly concentrated on the $15f_r$. The amplitude of f_r increases first and then remains at a certain level with the increasing error fluctuation and the mesh frequency's amplitude gradually increases, which is caused by the increasing error fluctuation. In addition, the region of continuous frequency becomes wider and the amplitude significantly increases. The chaotic behavior is clearly visible of the system. The numerical computations confirm the prediction of analytical chaos for applied value of e_r.
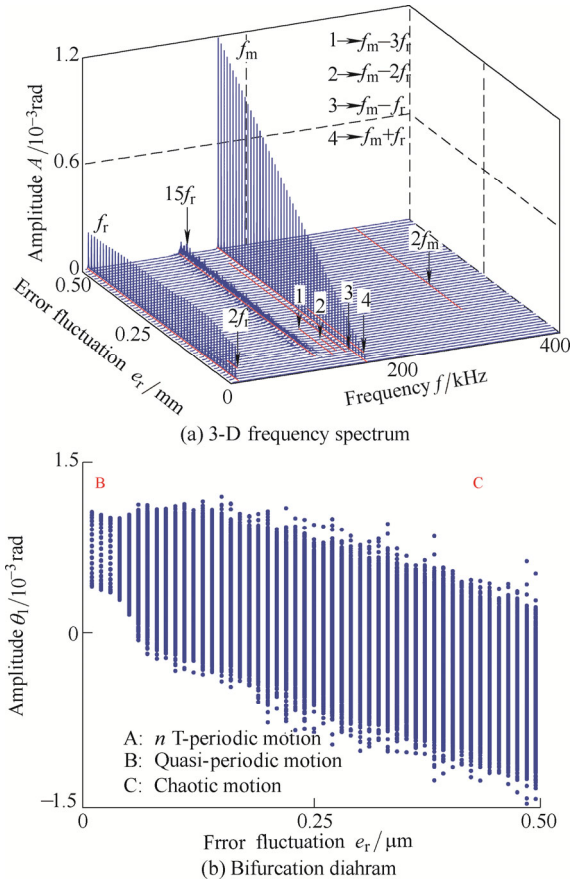
(a) 3-D frequency spectrum

(b) Bifurcation diahram

Fig. 11.　3-D frequency spectrum and bifurcation diagram

3.4　Analysis of the effect of the load fluctuation

In this section, a case study is analysed in order to understand the influences of load fluctuation on the dynamic behaviors. The effects of load fluctuation on dynamic responses are shown in Fig. 12(lightly fluctuation) and Fig. 13(heavily fluctuation) to highlight its influence on steady state response. As observed in Fig.12 for $T_{dr}=100$ N/m, the vibration displacement is periodic motion. In Fig. 12(b), the mesh frequency(f_m) component dominated frequency spectrum, and the amplitude of rotational frequency(f_r) is less than the mesh frequency's amplitude. The phase diagram exihibts regular motion in Fig. 12(c). The single-sided impact can be verified by Fig. 12(d). For heavy fluctuation case at $T_{dr}=500$ N/m, it can observe the rich nonlinear behaviors including coupled frequency and doubled-sided impact. In Fig. 13(a), the vibration displacement in y directon exhibits complicated harmonic components and seems as nonperiodic motion. The vibration amplitude increases with greater load fluctuation. The rotational frequency f_r dominated in spectrum and the amplitude of mesh frequency(f_m) is less than the rotational frequency's amplitude. In addition, the multiplication frequency(nf_r), the combination frequency($f_m\pm f_r$, $2f_m\pm f_r$) and continuous excitation frequency components can be observed obviously. The phase diagram is highly disordered in Fig. 13(c). Because of $\delta_{max}>b$ and $\delta_{min}<-b$, double-sided impact exists in the system. The results presented in Fig.13 indicate that the SGRBS undergoes different motions with changing load fluctuation condition.
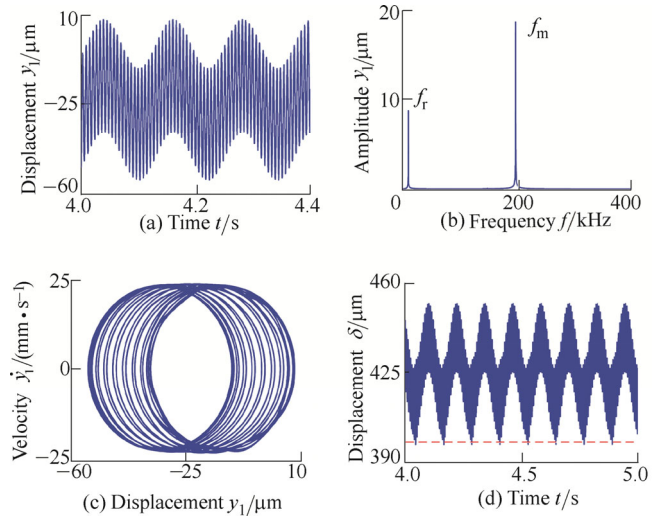

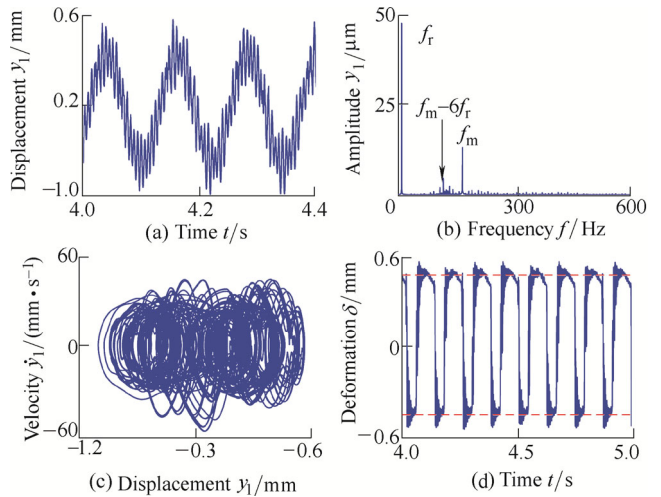Fig. 12.　Vibration responses of SGRBS at $T_{dr}=100$ N/m

Fig. 13.　Vibration responses of SGRBS at $T_{dr}=500$ N/m

Fig. 14 presents the dynamic mesh force at $T_{dr}=100$ N/m and $T_{dr}=500$ N/m. According to the simulation results, the load fluctuation can cause the stronger vibration of the mesh force. The SGRBS has a large deformation and crowded teeth phenomenon occur, which may cause the higher dynamic loads. The single-sided impact transits to doubled-sided impact.
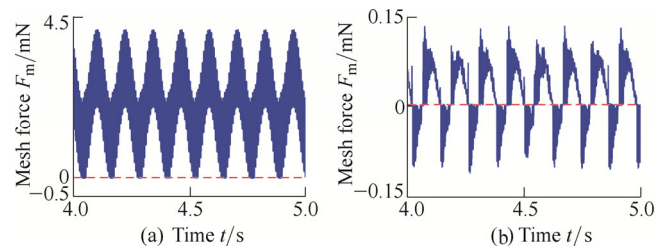

Fig. 14.　Mesh force at $T_{dr}=100$ N/m and $T_{dr}=500$ N/m

For a better clarity, Fig. 15 displays the 3-D frequency spectrum(Fig. 15(a)) and the bifurcation diagram(Fig. 15(b)) of the SGRBS using the load fluctuation T_{dr} as a control parameter at $\omega=500$ r/min. For light load fluctuation, i.e., $T_{dr}\leqslant 105$N/m, the SGRBS only exhibits two types of frequency components, namely, rotational frequency(f_r) and

• 290 •

ZHOU Shihua, et al: Nonlinear Dynamic Analysis of Coupled Gear-Rotor-Bearing System
with the Effect of Internal and External Excitations

mesh frequency(f_m). The mesh frequency dominated in 3-D frequency spectrum and the amplitude is considerably large than the amplitude of f_r. In addition, the amplitude of the f_m has an approximate constant and the amplitudes are approximately the same magnitude.

(a) 3-D frequency spectrum
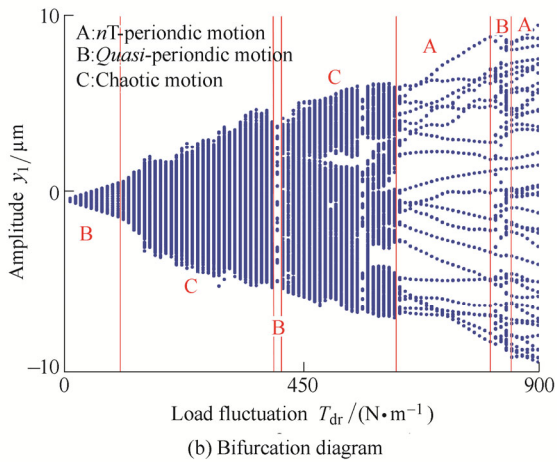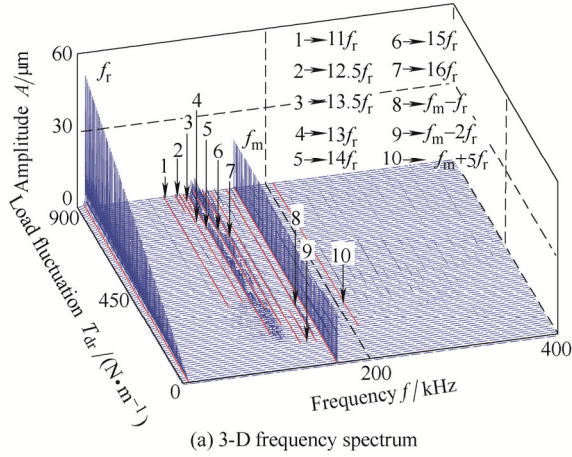

(b) Bifurcation diagram

Fig. 15.   3-D frequency spectrum and bifurcation diagram

As observed from Fig. 15(b), as T_{dr} increases, the nT-periodic motion transits to quasi-periodic motion. With the increase of the excitation force amplitude from 105 N/m to 395N/m, the 3-D frequency spectrum performs complicated frequency components, and the f_r and f_m are the dominated responses. Besides, the continuous frequency components mainly concentrated on the frequencies between $14f_r$ and $17f_r$. The amplitudes exist obvious difference among various frequencies, where the amplitude of f_r increases and the f_m increases first and then decreases gradually. In the corresponding bifurcation diagram, the system begins to execute the chaotic behavior. When the $T_{dr} \in [395, 405]$ N/m, the continuous frequency components gradually vanish and the nf_r is evident. The amplitude of f_r is also the dominated component and the f_m is the second largest after that of the rotational frequency f_r. In Fig. 15(b), the chaotic motion is replaced by quasi-periodic motion. As T_{dr} increases from 405N/m to 630N/m, the f_r, $14f_r$, $15f_r$, $f_m(20f_r)$ is the dominated vibration resopnses and the amplitudes of f_r and f_m increase

obviously, the amplitude of $14f_r$ increases with fluctuation. In addition, the region of continuous frequency becomes narrow and the multiplication frequency components (nf_r) appear clearly in 3-D frequency spectrum. The chaotic behavior can be seen as show in Fig. 15(b). For values of the load fluctuation in the range $T_{dr} \in [630, 805]$ N/m, the f_r, f_m and the multiplication frequency components(nf_r) can be observed significantly, especially the f_r, $14f_r$, $15f_r$, $16f_r$, f_m components. The amplitude of f_r is larger than the mesh frequency's amplitude and other frequency's amplitudes are relatively lesser, and thus it can be inferred that the system's behavior transits from chaotic to periodic motion with the changing T_{dr}. Finally, for all from $T_{dr} \geqslant 805$ N/m, the SGRBS performs rich frequency components, which contain the multiplication frequency and multiplication frequency components. The amplitude of f_r is obvious larger than other components, which illustrates the external excitation is the main influence than internal excitation. The dynamic behaviors of the gear system are found to be quasi-periodic motion at $T_{dr} \in [805, 835]$ and periodic motion at $T_{dr} \in [835, 900]$. The results indicate that the excitation force amplitude has an influence on the nonlinear dynamic characteristics and the increase of the excitation force amplitude makes the vibration amplitude increase but it may restrict the chaotic motion at some extent.

4   Conclusions

(1) An 8-DOF model of the SGRBS is presented in which the effects of the different parameters are studied and calculated. The results provide a detailed understanding of nonlinear dynamic behaviors under rotational speed, error fluctuation(internal excitation) and load fluctuation (external excitation) conditions, which enable suitable values of the key parameters to be specified such that chaotic behavior can be avoided and reducing the vibration and impact of the gear system.

(2) The rotational speed has significant influence on the nonlinear dynamic behaviors of the SGRBS. The system exhibits different motions such as periodic motion, quasi-periodic motion and chaotic motion under different rotational speed conditions. In addition, the no tooth impact, single-sided tooth impact, double-sided tooth impact and coupled lateral-torsional vibration of gear system can be clearly observed in 3-D frequency spectrum and bifurcation diagram.

(3) At relatively low error fluctuation, the rotational frequency amplitude is dominated response, which indicates that the external excitation is main excitation in the system. With the increase of the error fluctuation, the mesh frequency's amplitude is larger than others and the error fluctuation obviously has effect on the system's vibration and the internal excitation plays the leading role, which makes the system undergo chaotic behavior.

(4) The load fluctuation has a significant influence on the vibration response. It can be seen that, with the increase of

load fluctuation, the amplitude of f_r increases obviously and the nonlinear dynamic behaviors are corresponding with no tooth impact, single-sided tooth impact and double-sided tooth impact. The results indicate that the excitation force amplitude has an influence on the nonlinear dynamic characteristics and the increase of the excitation force amplitude makes the vibration amplitude increase but it may restrict the chaotic motion at some extent.

References

[1] KAHRAMAN A, SINGH R. Nonlinear dynamic of a spur gear pair[J]. *Journal of Sound and Vibration*, 1990, 142(1): 49–75.

[2] KAHRAMAN A, SINGH R. Interactions between time-varying mesh stiffness and clearance nonlinear in a geared system[J]. *Journal of Sound and Vibration*, 1991, 146(1): 135–156.

[3] LI Yinggang, CHEN Tianning, WANG Xiaopeng. Non-linear dynamics of gear pair with dynamic backlash subjected to combined internal and external periodic excitations[J]. *Journal of Vibration and Control*, 2014, 8(1): 1–11.

[4] BARBIERI M, BONORI G, PELLICANO F. Corrigendum to: Optimum profile modifications of spur gears by means of genetic algorithms[J]. *Journal of Sound and Vibration*, 2012, 331(21): 4825–4829.

[5] BONORI G, PELLICANO F. Non-smooth dynamics of spur gears with manufacturing errors[J]. *Journal of Sound and Vibration*, 2007, 306(1–2): 271–283.

[6] CHEN Siyu, TANG Jinyuan, LUO Caiwang, et al. Nonlinear dynamic characteristics of geared rotor bearing systems with dynamic backlash and friction[J]. *Mechanism and Machine Theory*, 2011, 46(4): 466–478.

[7] ZHOU Shihua, LIU Jie, LI Chaofeng, et al. Nonlinear behavior of a spur gear pair transmission system with backlash[J]. *Journal of Vibroengineering*, 2014, 16(8): 3850–3861.

[8] WEI Sha, ZHAO Jingshan, HAN Qinkai, et al. Dynamic response analysis on torsional vibrations of wind turbine geared transmission system with uncertainty[J]. *Renewable Energy*, 2015, 78: 60–67.

[9] ZHU Weilin, WU Shijing, WANG Xiaosun, et al. Harmonic balance method implementation of nonlinear dynamic characteristics for compound planetary gear sets[J]. *Nonlinear Dynamics*, 2015, 81(3): 1511–1522.

[10] WAN Cai, CHANG Jian. Bifurcation and chaos of gear-rotor-bearing system lubricated with couple-stress fluid[J]. *Nonlinear Dynamics*, 2015, 79(1): 749–763.

[11] MA Hui, PANG Xu, SONG Rongze, et al. Vibration response analysis of a geared rotor system considering the tip relief[J]. *Journal of Mechanical Engineering*, 2014, 50(7): 39–45. (in Chinese)

[12] MA Hui, YANG Jian, SONG Rongze. Effects of tip relief on vibration responses of a geared rotor system[J]. *Proceedings of the Institution of Mechanical Engineers, part C: Journal of Mechanical Engineering Sci*ence, 2014, 228(17): 1132–1154.

[13] FAGGIONI M, SAMANI F S, BERTACCHI G, et al. Dynamic optimization of spur gears[J]. *Mechanism and Machine Theory*, 2011, 46(4): 544–557.

[14] LEE A S, HA J W, CHOI D H. Coupled lateral and torsional vibration characteristics of a speed increasing geared rotor-bearing system[J]. *Journal of Sound and Vibration*, 2003, 263(4): 725–742.

[15] YASSINE D, AHMED H, LASSAAD W, et al. Effects of gear mesh fluctuation and defaults on the dynamic behavior of two-stage straight bevel system[J]. *Mechanism and Machine Theory*, 2014, 82: 71–86.

[16] HUANG Kuotao, WU Maorong, TSENG J T. Dynamic analyses of gear pairs incorporating the effect of time-varying lubrication damping[J]. *Journal of Vibration and Control*, 2011, 17(3): 355–363.

[17] STRINGER D B, SHETH P N, ALLAIRE P E. Modal reduction of geared rotor systems with general damping and gyroscopic effects[J]. *Journal of Vibration and Control*, 2011, 17(7): 975–987.

[18] HE S, CHO S M, SINGH R. Prediction of dynamic friction forces in spur gears using alternate sliding friction formulations[J]. *Journal of Sound and Vibration*, 2008, 309(3–5): 843–851.

[19] PAREY A, BADAOUI M E, GUILLET F, et al. Dynamic modelling of spur gear pair and application of empirical mode decomposition-based statistical analysis for early detection of localized tooth defect[J]. *Journal of Sound and Vibration*, 2006, 294(3): 547–561.

[20] OMAR F K, MOUSTAFA K A F, EMAM S. Mathematical modeling of gearbox including defects with experimental verification[J]. *Journal of Vibration and Control*, 2012, 18(9): 1310–1321.

[21] HOTAIT M A, KAHRAMAN A. Experiments on the relationship between the dynamic transmission error and the dynamic stress factor of spur gear pairs[J]. *Mechanism and Machine Theory*, 2013, 70: 116–128.

[22] TAMMINANA V K, KAHRAMAN A, VIJAYAKAR S. A study of the relationship between the dynamic factors and the dynamic transmission error of spur gear pairs[J]. *Journal of Mechanical Design*, 2007, 129(1): 75–84.

[23] AMARNATH M, CHANDRAMOHAN S, SEETHARAMAN S. Experimental investigations of surface e wear assessment of spur gear teeth[J]. *Journal of Vibration and Control*, 2012, 18(12): 1009–1024.

[24] LEE S K, AMARNATH M. Experimental investigations to establish correlation between stribeck curve, specific film thickness and statistical parameters of vibration and sound signals in a spur gear system[J]. *Journal of Vibration and Control*, 2014, 14(1): 1–15.

[25] WANG Cheng, CUI Yahui, ZHANG Qingping, et al. Modified optimization and experimental investigation of transmission error, vibration and noise for double helical gears[J]. *Journal of Vibration and Control*, 2014, 20(1): 1–13.

[26] RAFIQ M, CAN U, DOGRUER H, et al. Nonlinear dynamic modeling of gear-shaft-disk-bearing systems using finite elements and describing functions[J]. *Journal of Mechanical Design*, 2004, 126(3): 534–541.

[27] MA Hui, PANG Xu, ZENG Jin, et al. Effects of gear crack propagation paths on vibration responses of the perforated gear system[J]. *Mechanical Systems and Signal Processing*, 2015, 62-63: 113–128.

[28] MA Hui, ZENG Jin, FENG Ranjiao, et al. Review on dynamics of cracked gear systems[J]. *Engineering Failure Analysis*, 2015, 55: 224–245.

[29] MOHMMED O D, RANTATALO M, AIDANPAA J O. Dynamic modelling of a one-stage spur gear system and vibration-based tooth crack detection analysis[J]. *Mechanical Systems and Signal Processing*, 2015, 55: 293–305.

[30] HU Zehua, TANG Jinyuan, CHEN Siyu et al. Coupled translation-rotation vibration and dynamic analysis of face geared rotor system[J]. *Journal of Sound and Vibration*, 2015, 351: 282–298.

[31] ZHOU Changjiang, CHEN Siyu. Modeling and calculation of impact friction caused by corner contact in gear transmission[J]. *Chinese Journal of Mechanical Engineering*, 2014, 27(5): 958–964.

[32] CUI Yahui, LIU Zhansheng, YE Jianhuai. Dynamic response of geared rotor system and the effect of clearance on jump characteristics of amplitude[J]. *Journal of Mechanical Engineering*, 2009, 45(7): 7–15. (in Chinese)

Biographical notes

ZHOU Shihua, born in 1987, is a PhD candidate at *School of Mechanical Engineering and Automation, Northeastern University, China*. His research interest is the dynamic

• 292 •

ZHOU Shihua, et al: Nonlinear Dynamic Analysis of Coupled Gear-Rotor-Bearing System
with the Effect of Internal and External Excitations

characteristics of gear-rotor system and vehicle dynamics.
Tel: +86-18809884357; E-mail: zhou_shihua@126.com

SONG Guiqiu, born in 1960, is currently a professor at *Northeastern University, China*. He received his PhD degree from *Northeastern University, China*. His research interests include vehicle dynamics, fault diagnosis and machinery engineering theories.
Tel: +86-24-83674338; E-mail: guiqiusong@126.com

REN Zhaohui, born in 1968, is currently a professor at *Northeastern University, China*. He received his PhD degree from *Northeastern University, China*, in 2005. His research interests

include rotor dynamics, fault diagnosis and product integrated design method
Tel: +86-13889179917; E-mail: zhhren@mail.neu.edu.cn

WEN Bangchun, born in 1930, is currently a professor at *School of Mechanical Engineering and Automation, Northeastern University, China*. His main research interests include vibration utilization engineering, rotor dynamics, nonlinear vibration and applications of mechanical engineering, vibration diagnostics of the machine fault, mechanical-electronic integration and the machinery engineering theories.
Tel: +86-24-83674338; E-mail: bcw1930@mail.neu.edu.cn.